Check for updates

Co-doping effect of Mn^{2+} on fluorescence thermostability of Ca-α-sialon:Eu^{2+} phosphors

Jia Ni, [abc] Qian Liu,*[ab] Zhenzhen Zhou[ab] and Guanghui Liu[ab]

To reveal transition metal manganese ion (Mn^{2+}) co-doping influence on Ca-α-sialon:Eu^{2+} phosphors, Mn^{2+} and europium ion (Eu^{2+}) co-doped Ca-α-sialon phosphors were synthesized using a solid state reaction at 1600 °C under an ambient nitrogen atmosphere, and the effects of the co-dopant Mn^{2+} on the fluorescence thermostability of Ca-α-sialon:Eu^{2+} phosphors were systematically investigated. With increasing Mn^{2+} concentration, X-ray diffraction analysis shows a phase-pure host Ca-α-sialon structure and unit cell shrinkage (or a tighter structure). The photoluminescence spectra of all samples, with or without Mn^{2+} co-doping, exhibit a strong yellow emission. For the energy transfer between Mn^{2+} and Eu^{2+}, the emission intensity is strongest when the co-doping concentration of Mn^{2+} is 0.02 molar and the CIE chromaticity index of the strongest emission composition is (0.474, 0.513) with a high internal quantum efficiency of 72.4%. Importantly, the fluorescence thermal quenching behavior of the as-prepared phosphors is remarkable and is over 80% of the initial emission intensity tested at room temperature, at a higher temperature of 275 °C. The major energy transition mechanism between co-dopants Mn^{2+} and Eu^{2+} during the heating process was deduced and considered to be a non-radiative energy transfer and phonon-assisted tunneling. Using further calculations, the thermal activation energy, ΔE, is 0.28 eV. In consequence, Mn^{2+} and Eu^{2+} co-doped Ca-α-sialon is an attractive and competitive phosphor candidate for applications in white light emitting diodes.

1. Introduction

In the 1970s, α-sialon was first found and promised to be useful as a structural material, which stemmed from its solid solution feature of strong covalent silicon nitride (Si_3N_4).[1,2] By 2002, the research teams of Hintzen *et al.*[3] and Xie *et al.*[4] not only proposed that α-sialon could be applied to phosphor as a consolidus host material but also demonstrated its excellent luminescence properties, such as high thermal stability, high efficiency and a friendly environment.

In past decade, α-sialon, as a good silicon-based oxynitride host material has been attracting much attention and has been widely studied. The chemical formula of α-sialon is $M_{m/v}Si_{12-(m+n)}Al_{m+n}O_nN_{16-n}$ (where v is the valence of the M ion). In this composition, M consists of a compensation cation (calcium (Ca^{2+}), lithium (Li^+), magnesium (Mg^{2+}), strontium (Sr^{3+}), and so on)[5–7] and most rare earth metals (europium (Eu^{2+}), cerium (Ce^{3+}), terbium (Tb^{3+}), and so on).[4,7,8] The changes of the *m* and *n* values represent the quantity of (Si–N) bonds, (Al–N) bonds and (Al–O) bonds in M-α-sialon.[9–11] The ratio of these bonds exerts effects on the luminescence properties. In the previously mentioned systematic research, Eu^{2+} and Ce^{3+} doped Ca-α-sialon possess better luminescence properties. In a Ca-α-sialon host, activator Eu^{2+} and Ce^{3+} is 5d–4f transitions with a strong nephelauxetic effect and large ligand field splitting, showing a typical broad yellow and green emission with high thermal stability. They could keep ∼70% of the initial emission intensity when the temperature reached 300 °C, and this was far better than results obtained using yttrium aluminium garnet (YAG):Ce^{3+}.[12] Besides the wider emission wavelength range and high thermal stability, compared with other oxide and oxynitride phosphors (*e.g.*, $BaSi_3O_4N_2$,[13] $BaMgAl_{10}O_{17}$,[14] and so on), Eu^{2+} or Ce^{3+} doped Ca-α-sialon possesses a high external quantum efficiency (QE) of about 40%.[15,16] Furthermore, relative to nitride phosphors $CaAlSiN_3$[17] which have complex requirements to prepare, Ca-α-sialon phosphor is easier to prepare.

Currently, to achieve better luminescence properties of phosphors and low utilization of expensive rare earth elements, manganese (Mn^{2+}) used as a sensitizer was introduced in to many host materials co-doped with Eu^{2+} and this has been studied extensively.[18–21] It has been reported that the energy transfer between Mn^{2+} and Eu^{2+} is efficient with several phosphors, such as $Mg_2Al_4Si_5O_{18}$ and apatite-type fluorophosphate phosphors, and this could improve the emission intensity and influence the emission wavelength to red shift. Also, it has been

State Key Laboratory of High Performance Ceramics and Superfine Microstructure, Shanghai Institute of Ceramics, Chinese Academy of Sciences, 1295 Dingxi Road, Shanghai, 200050, China. E-mail: qianliu@mail.sic.ac.cn

Shanghai Materials Genome Institute, 99 Shangda Road, Shanghai 200444, China

University of Chinese Academy of Sciences, 19A Yuquan Road, Beijing 100049, China

determined from the previously mentioned papers that the energy transfer between the sensitizer Mn^{2+} and the activator Eu^{2+} is proportional to the spectral overlap between the emission band of the sensitizer and the excitation band of the acceptor. In accordance with the previous studies, the energy transfer between Eu^{2+} and Mn^{2+} in Ca-α-sialon is attributed to the resonance transfer under excitation in a room temperature (RT) environment.[22] However, much work is still needed to explore the Mn^{2+}/Eu^{2+} co-doped Ca-α-sialon to enrich the understanding of scientific recognition and to understand its practical applications.

In this research, Mn^{2+} and Eu^{2+} co-doped Ca-α-sialon was successfully prepared using a solid-state reaction. The effects of co-doped Mn^{2+} on the luminescence properties and especially on the thermal quenching behavior were investigated in detail. Furthermore, the energy transfer phenomenon between Eu^{2+} and Mn^{2+} under high temperature conditions was also considered and a non-radiative energy transfer and phonon-assisted tunneling mechanism was deduced.

2.   Experimental procedures

2.1   Synthesis of Ca-α-sialon:Eu^{2+},Mn^{2+} phosphors

The phosphors with the compositions of $Ca_{0.92-x}Si_9Al_3-ON_{15}$:$0.08Eu^{2+}$,$xMn^{2+}$ ($x = 0, 2, 4, 6, 8, 10$ mol%) were prepared using a traditional high temperature solid-state reaction method, with a fixed and optimal Eu^{2+} doping content of 0.08 mol based on previous research, and these were used to find out the Mn^{2+} co-doping influence on Ca-α-sialon:Eu^{2+} phosphors. The starting materials were α-Si_3N_4 (SN-E10, Ube Industries, Japan), aluminum nitride (AlN, Grade A, Starck Industries, Germany), calcium carbonate (≥99.90%, AR, Sinopharm Chemical Reagent Co., Ltd, China), europium(III) oxide (99.99%, Shanghai Yuelong New Materials Co., Ltd., Shanghai, China) and manganese(II) carbonate (CP, Sinopharm Chemical Reagent Co., Ltd, China). After mixing and grinding the powders thoroughly in an agate mortar for two h, the powdered mixture was put into BN crucibles, loaded in a graphite furnace, and finally calcined at 1600 °C for 4 h under a 0.8 L min^{-1} nitrogen (N_2) flow. The as-prepared powders were cooled down to RT in the furnace and ground finely again to obtain the final powders for further analysis.

2.2   Characterization

The products of synthesized powders were identified using X-ray powder diffraction (XRD, D8 ADVANCE, Bruker, Germany) with CuK$_α$ radiation ($λ = 0.1541$ nm). Photoluminescence (PL) spectra and temperature dependent luminescence properties (from 25 °C to 275 °C) were performed on a fluorescence spectrometer (F-4600, Hitachi, Japan) with a 150 W xenon lamp. The QE spectra were measured by using the integrated sphere on the time resolved and steady state fluorescence spectrophotometer (FLS980, Edinburgh Instruments, UK). The decay curves of the lifetime values were also recorded on the FLS 980 with a μF2 tunable microsecond flashlight (Edinburgh Instruments, UK), using a 450 W xenon lamp as excitation source, with pulsed

light, measured under a fixed wavelength of 570 nm emission and 375 nm excitation, simultaneously, combined with a time correlated single photon counting card and specialty software (Fluoracle, Edinburgh Instruments) to analyze and draw the decay curves.

3.   Results and discussion

3.1   Phase composition of Ca-α-sialon:Eu^{2+},Mn^{2+} phosphors

XRD patterns of Ca-α-sialon:$0.08Eu^{2+}$,xMn^{2+} phosphors are shown in Fig. 1a, with a standard reference pattern of Ca-α-sialon at the bottom. The intense and sharp crystal diffraction peaks indicate that all the samples agreed well with the structure of Ca-α-sialon (JCPDS 33-0261) and no visible impurity phases were detected. Compared with the phosphors without dopant Mn^{2+}, the diffraction peaks in the selected $2θ$ region from 33° to 36° gradually shift to higher $2θ$ angles with increasing Mn^{2+} concentration (seen in Fig. 1b), which is because of the lattice shrinking caused by smaller Mn^{2+} ions (0.067 nm ionic radius) substituting for larger Ca^{2+} ions (0.10 nm ionic radius). The previous experimental results show that the transition metal cation, Mn^{2+}, has been co-doped into the Ca-α-sialon:$0.08Eu^{2+}$ lattices.

3.2   Photoluminescence properties of Ca-α-sialon:Eu^{2+},Mn^{2+} phosphors

The excitation and emission PL spectra of two representative phosphors of Ca-α-sialon:$0.08Eu^{2+}$, and Ca-α-sialon:$0.08Eu^{2+}$,$0.02Mn^{2+}$ are shown in Fig. 2a. The spectra of both excitation and emission for the Mn^{2+} doped sample are identical to the spectra of the sample without Mn^{2+} dopant. The excitation spectra present two broad bands with maxima at ~287 nm and ~375 nm. The band of ~287 nm is attributed to the absorption of the Ca-α-sialon host lattice,[23] whereas the band of ~375 nm originates from the $4f^7 → 4f^65d$ electron transition of Eu^{2+}. The emission spectra only show one broad band and its center peak around ~570 nm is attributed to the energy transfer from the $4f^65d$ excited state to the $4f^7$ ground state of the Eu^{2+} rare earth ions.[23] The increased excitation spectrum of Ca-α-sialon:$0.02Mn^{2+}$ is also illustrated in Fig. 2a, and shows an obvious overlap between the emission spectrum of Ca-α-sialon:$0.08Eu^{2+}$ and the excitation spectrum of Ca-α-sialon:$0.02Mn^{2+}$, indicating the energy transfer interaction

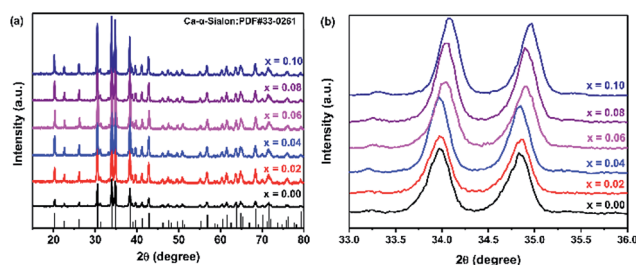**Fig. 1** (a) XRD patterns of Ca-α-sialon:$0.08Eu^{2+}$,xMn^{2+} phosphors with various Mn^{2+} concentrations ($x = 0.00-0.10$); (b) magnified regions of the XRD patterns in the $2θ$ range of 33–36°.
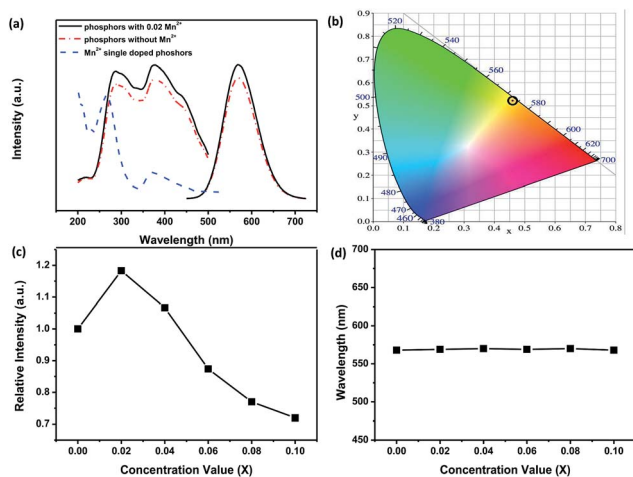
Fig. 2 (a) Excitation and emission spectra of Ca-α-sialon:0.08Eu^{2+}, Ca-α-sialon:0.08Eu^{2+},0.02Mn^{2+} phosphors, and the enlarged excitation spectrum of Ca-α-sialon:0.02Mn^{2+}. (b) CIE chromaticity diagram for Ca-α-sialon:0.08Eu^{2+} and Ca-α-sialon:0.08Eu^{2+},0.02Mn^{2+} phosphors under 375 nm excitation. (c) PL intensity of Ca-α-sialon:0.08Eu^{2+},xMn^{2+} (x = 0.00–0.10) around 570 nm emission as a function of Mn^{2+} concentration. (d) Emission peak wavelength of Ca-α-sialon:0.08Eu^{2+},xMn^{2+} (x = 0.00–0.10) as a function of Mn^{2+} concentration.

between Eu^{2+} and Mn^{2+}. In Fig. 2b, the Commission Internationale de l'Éclairage (CIE) chromaticity diagrams of the two phosphors, Ca-α-sialon:0.08Eu^{2+}, and Ca-α-sialon:0.08Eu^{2+},0.02Mn^{2+}, excited under 375 nm blue light are shown. The CIE chromaticity index for Ca-α-sialon:0.08Eu^{2+} is (0.473, 0.514) and for Ca-α-sialon:0.08Eu^{2+},0.02Mn^{2+} is (0.474, 0.513). It gives a distinct visual that the CIE chromaticity index of these two phosphors are very close and both of them belong to typical yellow phosphors which can be coupled to blue light-emitting diode (LED) chips for generating white light. Meanwhile, the internal QE of phosphors under 375 nm excitation were measured and calculated using the following expression:[24,25]

$$\eta_{QE} = \frac{\int L_s}{\int E_R - \int E_s} \quad (1)$$

where L_s is the emission spectra of the measured phosphors, E_R and E_s are the excitation spectra without and with the measured phosphors, respectively, in the integrating sphere. The internal η_{QE} value of Ca-α-sialon:0.08Eu^{2+},0.02Mn^{2+} phosphors is 72.4%, a little higher than the 69.44% of Ca-α-sialon:0.08Eu^{2+} phosphors without Mn^{2+} dopants. Fig. 2c shows the doping dependence of emission luminescence intensity for the samples with varied Mn^{2+} concentration co-doped with 0.08Eu^{2+} in Ca-α-sialon host material. The highest emission intensity belongs to the as-prepared sample with a co-doping composition of x = 0.02 and then the emission intensity tends to decline with increased Mn^{2+} concentration, however, the emission intensity of Ca-α-sialon:0.08Eu^{2+},0.04Mn^{2+} phosphor is also stronger than that of the phosphor without Mn^{2+} dopants. This implies that there

exists some energy transfer interactions between Eu^{2+} and Mn^{2+}, which can be proved by the evidence of spectral overlap between the PL spectrum of Eu^{2+} and the photoluminescence excitation (PLE) spectrum of Mn^{2+} shown in Fig. 2a. In addition, the critical distance, R_c is also an important parameter to demonstrate the energy transfer. Researchers usually use eqn (2) to calculate R_c:[26,27]

$$R_c = 2(3V/4\pi Nx_c)^{1/3} \quad (2)$$

Using eqn (2), V is the volume of the unit cell of Ca-α-sialon (304.8 Å^3), N is the number of Z ions in the single unit cell (1), and x_c is the stoichiometric doping composition sum of the Eu^{2+} concentration of 0.08 and the Mn^{2+} critical concentration of 0.02 (assumed from Fig. 2c). Therefore, the calculated R_c is 17.98 Å. If the doping concentration of Mn^{2+} increases to 0.06 and 0.10, the value of R becomes smaller (16.08 Å and 14.78 Å, respectively). Therefore, with the further increase of Mn^{2+} content beyond 0.02 (after the second dot in the curve as shown in Fig. 2c), the critical distance R_c or the distance between the Mn^{2+} and Eu^{2+} decreases, resulting in an enhanced energy transfer interaction and the final concentration quenching of emission or emission intensity decline. It should be noted that the added Mn^{2+} composition is volatile to some extent during the high temperature calcination of phosphors, and the real content of Mn^{2+} in the prepared phosphors is below the stoichiometric composition and then the calculated critical distance R_c is rather smaller. Furthermore, based on the calculated R_c (more than 5–8 Å), the energy transfer model between Eu^{2+} and Mn^{2+} can be deduced as being multipolar interactions following Dexter's principle. In Fig. 2d, the emission peak positions of the Ca-α-sialon:0.08Eu^{2+} phosphors with different Mn^{2+} concentrations are tiny, and fluctuate around 570 nm and have no distinct emission shift. Therefore, the appropriate co-doping of Mn^{2+} with Eu^{2+} in the Ca-α-sialon host material can enhance the emission intensity and the internal QE as well, but does not induce the red shift of the emission at RT.

In general, the $^4T_1(^4G) \rightarrow {}^6A_1(^6S)$ transition of Mn^{2+} within the 3d shell strongly depends on lattice vibration and crystal field strength. In previous studies, the emission spectra of Mn^{2+} shows a broad green emission band in oxide hosts with tetrahedral coordination, whereas it emits orange to red light with octahedral coordination. Whereas, because of the strong nephelauxetic effect, it can also give red light (~600 nm) with tetrahedral coordination in AlN and AlON nitride hosts.[19,28,29] Furthermore, the dopant Mn^{2+} in Ca-α-sialon:0.08Eu^{2+} is expected to substitute for Ca^{2+} sites which are coordinated by seven (O, N) anions at three different M–(O, N) distances.[8,30,31] Theoretically speaking, the introduction Mn^{2+} in Ca-α-sialon:0.08Eu^{2+} can result in a red shift of the emission wavelength. However, in these experiments, the dopant Mn^{2+} in Ca-α-sialon:0.08Eu^{2+} only enhances the luminescence intensity observed from the spectra (Fig. 2c and d), and obvious emission shift is absent. It was supposed that $^4T_1 \rightarrow {}^6A_1$ d–d electron transition of Mn^{2+} is spin and parity-forbidden, compared to the 4f $\rightarrow$ 5d transition of Eu^{2+}, therefore, the emission intensity of the Mn^{2+}

ion singly doped phosphor is far weaker than that of the Eu^{2+} ion in many host materials,[32] as is the situation in the Ca-α-sialon host. In addition, the excitation wavelength of longer than the 375 nm selected in the experiments is probably not an appropriate excitation wavelength for Mn^{2+} emitting in Ca-α-sialon, and this is supported by the curves shown in Fig. 3, which show a stronger emission of Mn^{2+} centered at ∼600 nm under excitation of wavelengths shorter than 265 nm, rather than under excitation of a longer wavelength of 375 nm.

3.3 Thermal quenching behaviors of Ca-α-sialon:Eu^{2+},Mn^{2+} phosphors

In this research, the temperature dependent luminescent intensity of Ca-α-sialon:$0.08Eu^{2+}$ with ($x = 0.02$) and without Mn^{2+} was measured at a wider temperature range from RT (25 °C) to 275 °C and the results are shown in Fig. 4a. Because of the thermal quenching, the trend of the PL intensity trends to decline. The thermal quenching is ascribed to the non-radiative energy transfer and expressed in the schematic configuration coordinate diagram of Eu^{2+} and Mn^{2+} electrons in Ca-α-sialon lattice to describe the energy transfer process, as shown in Fig. 4b. In the configuration coordinate diagram, the lower parabola (black line) and higher two parabolas (green lines) represent the total energy of the ground state and excited states of Eu^{2+} and Mn^{2+}, respectively. In general, the electrons jump from the bottom of the ground state (black) to the Eu^{2+} and Mn^{2+} excited states (green) under 375 nm excitation, then the excited electrons partly release energy by radiative transition directly and vertically from the bottom of two excited states of Eu^{2+} and Mn^{2+} parabolas (green) to the bottom of the ground state (black) accompanied by yellow (575 nm) and red (600 nm) light emission. When heating the samples, except in the previously described process, part of the electrons obtains much more energy and reaches the high cross points P1 and P2 *via* the Eu^{2+} and Mn^{2+} parabola (green) and then transits to the bottom of the ground state *via* the ground state parabola (black). This is the non-radiative energy transfer and it is the major energy transfer during the whole heating process, and as
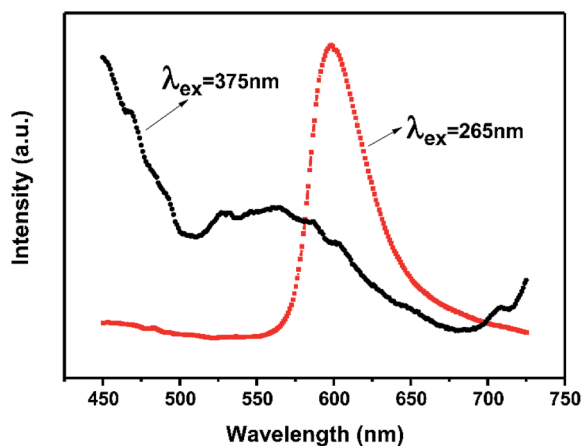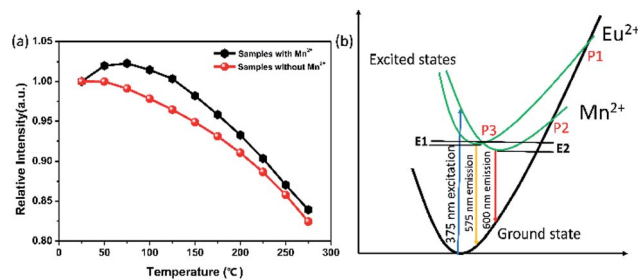

Fig. 4 (a) Temperature dependent luminescence of Ca-α-sialon: $0.08Eu^{2+}$ with ($x = 0.02$) and without Mn^{2+} phosphors measured under 375 nm excitation. (b) Schematic illustration of the configuration coordinate diagram of energy transfer in the Ca-α-sialon: $0.08Eu^{2+},0.02Mn^{2+}$ phosphor.

a result, the luminescence intensity is gradually weakened. From Fig. 4a, it is worth noting that the introduction of Mn^{2+} enhances rather than weakens the emission intensity of the phosphor at temperatures lower than 125 °C. From another perspective, the enhanced emission intensity should be considered as the phonon-assisted tunneling effect. At relatively low heating temperatures (<125 °C), by absorbing the extra heat energy, part of the heat excited electrons (also called phonons) move from the bottom of the low energy excited states (Mn^{2+}, green parabola) to the high energy excited states (Eu^{2+}, green parabola) *via* the cross point P3,[33] and finally release the obtained energy by radiatively emitting light. Consequently, the emission intensity enhancement occurs at relatively low heating temperatures by the phonon-assisted tunneling effect caused by the heating excitation. If the heating temperature increases further to high levels, the electrons could gain more energy and reach the high cross points, P1 and P2, *via* the Eu^{2+} and Mn^{2+} parabola (green) and then transit to the bottom of the ground state *via* the ground state parabola (black). This is described as non-radiative energy transfer or thermal quenching.

From the measured spectra, illustrated in Fig. 5a and b, the emission peak wavelengths of Ca-α-sialon:$0.08Eu^{2+},0.02Mn^{2+}$ shift from the long wavelength of 573 nm to the short wavelength of 567 nm with the increase of the heating temperatures, while the emission peak wavelengths of the single doped Ca-α-sialon:$0.02Mn^{2+}$ remain almost unchanged at around 573 nm. Otherwise, the slight decrease of the x values and the increase of y values in the chromaticity index, indicated in both Fig. 5c and Table 1, show more direct evidence of the emission blue-shift behavior of Ca-α-sialon:$0.08Eu^{2+},0.02Mn^{2+}$ with the increase in temperature. It has to be noted that this blue-shift of emission is caused partially by phonon-assisted tunneling.[33,34] From Fig. 4b, it can be seen that at first, although the energy barrier, E1, can be overcome, it is higher than E2, so the low energy emission of Mn^{2+} plays the major role in the reaction. When the temperature rises to a higher level, the thermal quenching energy goes over the E2 barrier and the high energy emission of Eu^{2+} gradually becomes dominant. Furthermore, in Table 1, the CIE chromaticity coordinate index of Ca-α-sialon: $0.08Eu^{2+},0.02Mn^{2+}$ phosphor, shift from (0.473, 0.514) at 25 °C
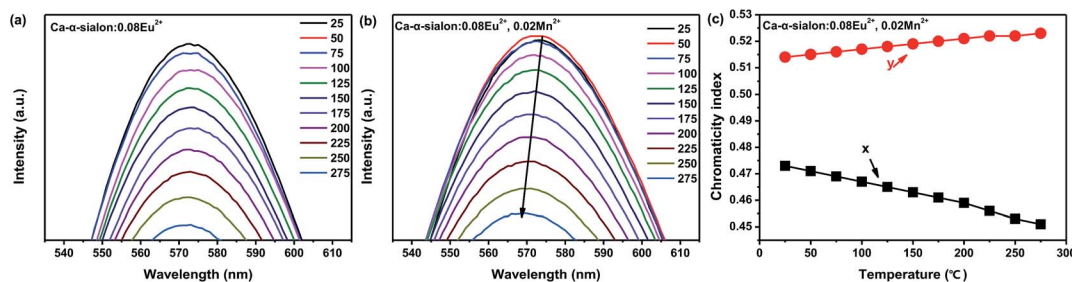

Fig. 3 Emission spectra of Ca-α-sialon:$0.02Mn^{2+}$ phosphors under excitation of 375 nm and 265 nm.

Fig. 5 (a) and (b) PL emission spectra of Ca-α-sialon:0.08Eu^{2+} without and with Mn^{2+} phosphors ($x = 0.02$) as a function of temperature. (c) CIE chromaticity coordinates of Ca-α-sialon:0.08Eu^{2+},0.02Mn^{2+} phosphor versus temperature.

to (0.451, 0.523) at 275 °C. This tiny displacement reveals the strong color stability of the co-doped phosphor.

However, in practical applications, phosphors are packed with LED chips when applied in solid-state lighting and the heat generated by LED chips always affects the emission intensity of phosphors during the service time. In terms of the LED industry standard, 150 °C is regarded as the working temperature for a high power white-LED (W-LED). For this standard, thermal stability under 150 °C becomes one of the crucial phosphor parameters. When the temperature reaches 150 °C, the emission intensity of Ca-α-sialon with ($x = 0.02$) and without Mn^{2+} maintains 98% and 94% of the initial intensity (RT), respectively, (see Fig. 4a), indicating that both of them have an excellent resistibility to thermal quenching and have a good thermal stability. As the working temperature rises to 275 °C, the emission loss of these two phosphors is less than 20% of the initial intensity (RT) and in thermal quenching behavior of the phosphors with Mn^{2+} co-doping are little better. To better understand the temperature dependence of the PL, the thermal activation energy for thermal quenching has been calculated according to the Arrhenius equation:[35,36]

$$I_0/I(T) = 1 + A \exp(-\Delta E/K_B T) \quad (3)$$

where I_0 is the initial PL intensity at RT, $I(T)$ is the PL intensity at a given temperature, A is a constant, ΔE is the activation energy for thermal quenching, and K_B is Boltzmann's constant (8.617 ×

10^{-5} eV K^{-1}). Based on eqn (3), the plot of ln[$I_0/I(T) - 1$] versus ($-1/K_B T$) has a linear relationship. Using the slope of the plot in Fig. 6, the best activation energy ΔE obtained is 0.28 eV for the phosphors with Mn^{2+} ($x = 0.02$) and the ΔE value is much larger than 0.24 eV for the phosphors without Mn^{2+}. Both of them are better than the thermal activation energy of commonly used commercial phosphor YAG:Ce^{3+} (0.189 eV).[37] The calculated results are in agreement with the experimental results and show that the co-dopant Mn^{2+} plays an important part in the thermal quenching property of Ca-α-sialon:Eu^{2+} phosphors.

3.4 Fluorescence decay

Fig. 7 shows the decay curves for three samples: single doped Ca-α-sialon:0.08Eu^{2+}, co-doped samples Ca-α-sialon:0.08Eu^{2+},0.02Mn^{2+} and Ca-α-sialon:0.08Eu^{2+},0.04Mn^{2+}, measured simultaneously with a fixed emission wavelength of 570 nm and excitation wavelength of 375 nm. All the experimental values can be fitted using the double-exponential equation:

$$I(t) = A_1 \exp(-t/\tau_1) + A_2 \exp(-t/\tau_2) \quad (4)$$

In eqn (4), I is the luminescence intensity, A_1 and A_2 are constants, t is the testing time, τ_1 and τ_2 are the shorter and longer decay times calculated using eqn (4). According to eqn (4) and using computerized fitting, the τ_1 and τ_2 results for the

Table 1 CIE chromaticity coordination values for Ca-α-sialon:0.08Eu^{2+},0.02Mn^{2+} phosphor versus temperature

Temperature (°C)	Chromaticity index x	Chromaticity index y
25	0.473	0.514
50	0.471	0.515
75	0.469	0.516
100	0.467	0.517
125	0.465	0.518
150	0.463	0.519
175	0.461	0.520
200	0.459	0.521
225	0.456	0.522
250	0.453	0.522
275	0.451	0.523
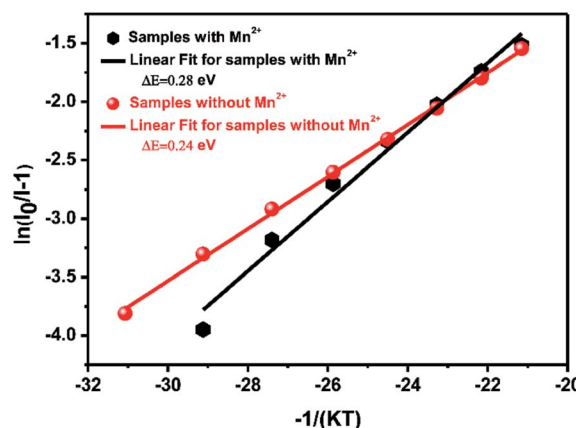
Fig. 6 Activation energy ΔE of thermal quenching of Ca-α-sialon:0.08Eu^{2+} with ($x = 0.02$) and without Mn^{2+} phosphors.
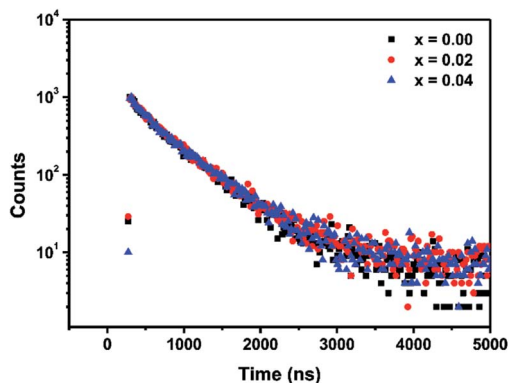
Fig. 7 Decay curves of three phosphor samples: Ca-α-sialon: $0.08Eu^{2+}$ (black dots), Ca-α-sialon:$0.08Eu^{2+},0.02Mn^{2+}$ (red dots) and Ca-α-sialon:$0.08Eu^{2+},0.04Mn^{2+}$ (blue dots), detected at $\lambda_{em} = 570$ nm and $\lambda_{ex} = 375$ nm.

Table 2 The calculation results of short decay time, long decay time and average decay time for Ca-α-sialon:$0.08Eu^{2+}$, Ca-α-sialon:$0.08Eu^{2+},0.02Mn^{2+}$ and Ca-α-sialon:$0.08Eu^{2+},0.04Mn^{2+}$ phosphors

Doping content	τ_1 (ns)	τ_2 (ns)	τ (ns)
$(0.08Eu^{2+})$	156.5	553.8	515.1
$(0.08Eu^{2+},0.02Mn^{2+})$	237.4	584.0	521.9
$(0.08Eu^{2+},0.04Mn^{2+})$	151.7	562.3	519.4

three samples are listed in Table 2. Furthermore, the average lifetime constant (τ) can be estimated as follows:

$$\tau = \frac{A_1\tau_1^2 + A_2\tau_2^2}{A_1\tau_1 + A_2\tau_2} \quad (5)$$

It is found that the average decay time of the sample with single Eu^{2+} doping is a little faster than that of the co-doped samples with 0.02 and 0.04 Mn^{2+} addition. In addition, the double-exponential decay indicates the existence of two relaxation processes. The fast decay components (τ_1) are defined by the PL intensity decay, whereas the slow decay components possibly result from the luminescence caused by defects of phosphors on the surface and inside.[38]

4. Conclusions

In summary, Mn^{2+} and Eu^{2+} co-activated Ca-α-sialon phosphors were prepared using a conventional high temperature solid-state reaction method. The prepared phosphors display intense yellow emission centered at 570 nm under 375 nm excitation and the optimal doping concentration of Mn^{2+} is $x = 0.02$ molar for all the Ca-α-sialon:$0.08Eu^{2+},xMn^{2+}$ compositions. Compared to Eu^{2+} single doped Ca-α-sialon, the increase of emission intensity indicates that additional energy transfer occurs between Eu^{2+} and Mn^{2+} during the luminescence process in the co-doped phosphors. The effective energy transfer leads to a good resistance behavior to thermal quenching. At 150 °C it can maintain 98% of the initial emission intensity (measured at

RT), and its emission intensity remains at over 80% when the temperature rises to 275 °C. Based on the calculation results, the thermal activation energy ΔE (0.28 eV) of the co-doped phosphors is larger than that of phosphor without Mn^{2+}. All the results show that the co-dopant Mn^{2+} plays a promoting role in the resistance to thermal quenching of the Ca-α-sialon:Eu^{2+} phosphors.

Conflicts of interest

There are no conflicts to declare.

Acknowledgements

Notes and references

1 K. H. Jack and W. I. Wilson, *Nature, Phys. Sci.*, 1972, **238**, 28–29.

2 Y. Oyama and O. Kamigait, *Jpn. J. Appl. Phys.*, 1971, **10**, 1637.

3 J. W. H. van Krevel, J. W. T. van Rutten, H. Mandal, H. T. Hintzen and R. Metselaar, *J. Solid State Chem.*, 2002, **165**, 19–24.

4 R.-J. Xie, M. Mitomo, K. Uheda, F.-F. Xu and Y. Akimune, *J. Am. Ceram. Soc.*, 2002, **85**, 1229–1234.

5 R.-J. Xie, N. Hirosaki, M. Mitomo, K. Sakuma and N. Kimura, *Appl. Phys. Lett.*, 2006, **89**, 241103.

6 S. Hampshire, H. K. Park, D. P. Thompson and K. H. Jack, *Nature*, 1978, **274**, 880–882.

7 R. J. Xie, N. Hirosaki, M. Mitomo, K. Uheda, T. Suehiro, X. Xu, Y. Yamamoto and T. Sekiguchi, *J. Phys. Chem. B*, 2005, **109**, 9490–9494.

8 Z. Shen, M. Nygren and U. Halenius, *J. Mater. Sci. Lett.*, 1997, **16**, 263–266.

9 R.-J. Xie, N. Hirosaki, M. Mitomo, T. Suehiro, X. Xu and H. Tanaka, *J. Am. Ceram. Soc.*, 2005, **88**, 2883–2888.

10 L. Liu, R.-J. Xie, N. Hirosaki, T. Takeda, J. Li and X. Sun, *J. Am. Ceram. Soc.*, 2009, **92**, 2668–2673.

11 K. Shioi, N. Hirosaki, R.-J. Xie, T. Takeda and Y. Q. Li, *J. Alloys Compd.*, 2010, **504**, 579–584.

12 R.-J. Xie and N. Hirosaki, *Sci. Technol. Adv. Mater.*, 2007, **8**, 588–600.

13 D. Huang, Y. Zhou, W. Xu, K. Wang, Z. Liu and M. Hong, *J. Alloys Compd.*, 2015, **653**, 148–155.

14 K.-B. Kim, Y.-I. Kim, H.-G. Chun, T.-Y. Cho, J.-S. Jung and J.-G. Kang, *Chem. Mater.*, 2002, **14**, 5045–5052.

15 R.-J. Xie, N. Hirosaki, M. Mitomo, K. Takahashi and K. Sakuma, *Appl. Phys. Lett.*, 2006, **88**(10), 101104.

16 L. Liu, X. Zhou, R.-J. Xie and Q. Huang, *Chin. Sci. Bull.*, 2012, **58**, 708–712.

17 B. Dierre, T. Takeda, T. Sekiguchi, T. Suehiro, K. Takahashi, Y. Yamamoto, R.-J. Xie and N. Hirosaki, *Sci. Technol. Adv. Mater.*, 2013, **14**, 064201.

18 J. Chen, Y. Liu, M. Fang and Z. Huang, *Inorg. Chem.*, 2014, **53**, 11396–11403.

19 X. J. Wang, R. J. Xie, B. Dierre, T. Takeda, T. Suehiro, N. Hirosaki, T. Sekiguchi, H. Li and Z. Sun, *Dalton Trans.*, 2014, **43**, 6120–6127.

20 N. Guo, C. Jia, J. Li, Y. Zhao, R. Ouyang, W. Lü and A. Setlur, *J. Am. Ceram. Soc.*, 2015, **98**, 1162–1168.

21 S. Miao, Z. Xia, J. Zhang and Q. Liu, *Inorg. Chem.*, 2014, **53**, 10386–10393.

22 Y.-q. Zhang, X.-j. Liu, Z.-r. Huang, J. Chen and Y. Yang, *J. Lumin.*, 2012, **132**, 2561–2565.

23 R.-J. Xie, N. Hirosaki, K. Sakuma, Y. Yamamoto and M. Mitomo, *Appl. Phys. Lett.*, 2004, **84**, 5404–5406.

24 W. A. Thornton, *J. Electrochem. Soc.*, 1969, **116**, 286–298.

25 K. Ohkubo and T. Shigeta, *Journal of the Illuminating Engineering Institute of Japan*, 1999, **83**, 87–93.

26 G. Blasse and A. Bril, *Philips Res. Rep.*, 1968, **23**, 201–206.

27 G. Blasse and W. Wanamaker, *Philips Res. Rep.*, 1968, **23**, 189.

28 B. Liu, Y. Wang, Y. Wen, F. Zhang, G. Zhu and J. Zhang, *Mater. Lett.*, 2012, **75**, 137–139.

29 R.-J. Xie, N. Hirosaki, X.-J. Liu, T. Takeda and H.-L. Li, *Appl. Phys. Lett.*, 2008, **92**, 201905.

30 F. Izumi, M. Mitomo and J. Suzuki, *J. Mater. Sci. Lett.*, 1982, **1**, 533–535.

31 G. Z. Cao and R. Metselaar, *Chem. Mater.*, 1991, **3**, 242–252.

32 Q. Guo, L. Liao, L. Mei and H. Liu, *J. Solid State Chem.*, 2015, **232**, 102–107.

33 H. Zhou, Q. Wang and Y. Jin, *J. Mater. Chem. C*, 2015, **3**, 11151–11162.

34 S. J. Gwak, P. Arunkumar and W. B. Im, *J. Phys. Chem. C*, 2014, **118**, 2686–2692.

35 S. Bhushan and M. V. Chukichev, *J. Mater. Sci. Lett.*, 1988, **7**, 319–321.

36 R.-J. Xie, N. Hirosaki, N. Kimura, K. Sakuma and M. Mitomo, *Appl. Phys. Lett.*, 2007, **90**, 191101.

37 C.-C. Chung and J.-H. Jean, *Mater. Chem. Phys.*, 2010, **123**, 13–15.

38 W. Zhou, S. Deng, C. Rong, Q. Xie, S. Lian, J. Zhang, C. Li and L. Yu, *RSC Adv.*, 2013, **3**, 16781.